

Grid Operational Benefit Analysis of Data Center Spatial Flexibility: Congestion Relief, Renewable Energy Curtailment Reduction, and Cost Saving

Haoxiang Wan

*Department of Electrical and Computer Engineering
University of Houston
Houston, TX, USA
hwan6@cougarnet.uh.edu*

Linhan Fang

*Department of Electrical and Computer Engineering
University of Houston
Houston, TX, USA
lfang7@cougarnet.uh.edu*

Xingpeng Li

*Department of Electrical and Computer Engineering
University of Houston
Houston, TX, USA
xli83@central.uh.edu*

Abstract—Data centers are facilities housing computing infrastructure for processing and storing digital information. The rapid expansion of artificial intelligence is driving unprecedented growth in data center capacity, with global electricity demand from data centers projected to double by 2026. This growth creates substantial challenges for power transmission networks, as large concentrated loads can cause congestion and threaten grid reliability. Meanwhile, the intermittent nature of solar and wind generation requires flexible resources to maintain grid reliability and minimize curtailment. This paper assesses whether data center spatial flexibility—the ability to migrate computational workloads geographically—can serve as a grid resource to address these challenges. An optimal power flow model is developed to co-optimize generation dispatch, security reserves, and flexible data center loads. Case studies on a modified IEEE 73-bus system show that inflexible data center placement can lead to severe transmission violations, with line overloads reaching 30.1%. Enabling spatial flexibility mitigates these violations in the studied scenarios and restores system feasibility. This flexibility also reduces solar curtailment by up to 61.0% by strategically reallocating load to solar-rich areas. The results suggest that spatial flexibility offers a viable approach to defer transmission upgrades and enhance renewable utilization.

Index Terms—Data center spatial flexibility, demand-side flexibility, locational marginal pricing, optimal power flow, renewable integration, transmission congestion

I. INTRODUCTION

The proliferation of artificial intelligence and big data analytics has catalyzed substantial growth in data center (DC) infrastructure, both in number and scale [1]. This expansion has contributed to rising energy consumption, with global data centers currently accounting for approximately 3% of total electricity supply [2]. The integration of these large, geographically concentrated loads into power transmission networks presents challenges for operational stability and capacity management. Concurrently, efforts to mitigate carbon emissions and diversify energy portfolios have accelerated the grid integration of renewable energy sources [3], introducing additional operational complexities.

The increasing deployment of variable renewable energy sources has introduced new dimensions to power system operations, particularly in transmission congestion management and economic dispatch optimization [4]–[6]. Recent advances in machine learning-based optimal power flow (OPF) formu-

lations have further expanded this field by enhancing computational efficiency and incorporating system-level constraints such as frequency stability and network congestion [7], [8]. According to Lawrence Berkeley National Laboratory's 2024 report, data centers consumed approximately 4.4% of total U.S. electricity in 2023, with projections indicating growth to 6.7–12% by 2028 [9]. This rapid expansion, driven by AI applications, manufacturing growth, and electrification initiatives, introduces geographically concentrated loads that may intensify transmission stress and contribute to locational marginal price (LMP) volatility [10], [11]. Addressing these challenges may require approaches that extend beyond conventional transmission expansion, which often involves substantial capital expenditures and extended implementation timelines [12].

Traditional congestion mitigation relies primarily on physical infrastructure investments such as transmission upgrades and energy storage deployment, each involving considerable capital costs and multi-year development cycles [13]. Demand-side management offers a complementary approach by leveraging load flexibility to potentially defer or reduce infrastructure requirements [14], [15]. However, existing frameworks have predominantly focused on temporal flexibility, with limited investigation of spatial flexibility—the strategic redistribution of computational workloads across geographically dispersed facilities. Data centers may present opportunities in this regard: their distributed architectures and delay-tolerant workloads can enable workload migration across locations with relatively minimal service impact, potentially functioning as spatially controllable demand resources [16].

Recent literature has examined data center participation in ancillary services and demand response programs [14]–[16], generally treating data centers as localized flexible loads. However, the potential for these facilities to serve as network-aware assets capable of influencing transmission congestion through spatial workload reallocation remains relatively unexplored. While Fridgen et al. [17] demonstrated the economic viability of spatial load migration for balancing power provision across international markets, spatial flexibility not only mitigates localized congestion but can also reshape power flow distributions at the system level, exerting a more

direct influence on renewable energy utilization and price stability. The concept of demand-side resources providing transmission-like services, where spatial load redistribution can substitute for or complement physical network capacity, has received limited systematic investigation. Existing studies have not sufficiently examined the technoeconomic role of data center spatial flexibility in mitigating renewable curtailment, alleviating transmission congestion, and reducing locational marginal price variability within integrated optimal power flow frameworks.

This paper presents an optimal power flow framework that models spatially flexible data centers and evaluates their potential role in alleviating transmission congestion and renewable curtailment. Using a modified IEEE 73-bus test system with distributed data center capacity and high solar penetration, the analysis examines four operational scenarios to address several interrelated questions: how inflexible deployment influences transmission feasibility under varying load conditions, whether spatial flexibility can restore system operability without physical network expansion, what transfer capability thresholds are required for congestion mitigation, and to what extent demand-side flexibility may reduce solar curtailment in transmission-constrained systems. The proposed framework identifies critical feasibility thresholds, economic saturation points, and curtailment reduction potential through systematic case studies. The findings suggest that spatial reallocation of data center loads can offer operational benefits; however, practical implementation would necessitate consideration of market design and coordination challenges beyond the scope of this study.

II. FORMULATION OF THE OPTIMIZATION MODEL

This section details the integrated optimization model that co-optimizes conventional generation, security reserves, renewable resources, and flexible demand within an OPF framework.

A. Objective Function

The objective minimizes total operational cost:

$$\min \sum_{g \in \mathcal{G}} c_g P_g, \quad (1)$$

where P_g and c_g denote the active power dispatch and marginal cost for generator $g \in \mathcal{G}$.

B. Network and Generation Constraints

Conventional generation is bounded by capacity limits:

$$P_g^{\min} \leq P_g \leq P_g^{\max}, \quad \forall g \in \mathcal{G}, \quad (2)$$

where P_g is the real power output of generator g , P_g^{\min} and P_g^{\max} are minimum and maximum capacity limits, and \mathcal{G} is the set of all generators.

Under Direct Current power flow approximation, active power flow P_k on branch $k \in \mathcal{K}$ is:

$$P_k = \frac{\theta_{f(k)} - \theta_{t(k)}}{x_k}, \quad \forall k \in \mathcal{K}, \quad (3)$$

where \mathcal{K} is the set of transmission branches, $\theta_{f(k)}$ and $\theta_{t(k)}$ are voltage angles at the from-bus and to-bus terminals, x_k is the series reactance, and $f(k), t(k)$ map branches to buses in set \mathcal{N} .

Branch flows are constrained by thermal ratings:

$$-\text{RateA}_k \leq P_k \leq \text{RateA}_k, \quad \forall k \in \mathcal{K}, \quad (4)$$

where RateA_k is the thermal capacity limit of branch k .

Nodal power balance at bus $n \in \mathcal{N}$ is:

$$\begin{aligned} \sum_{g \in \mathcal{G}(n)} P_g + P_n^{\text{solar}} + \sum_{k \in \mathcal{K}^-(n)} P_k - \sum_{k \in \mathcal{K}^+(n)} P_k \\ = d_n + L_n^{\text{optimized}}, \quad \forall n \in \mathcal{N}, \end{aligned} \quad (5)$$

where $\mathcal{G}(n)$ is the set of generators at bus n , P_n^{solar} is dispatched solar generation, $\mathcal{K}^-(n)$ and $\mathcal{K}^+(n)$ are branches flowing into and out of bus n , d_n represents the traditional inelastic electrical load, and $L_n^{\text{optimized}}$ denotes the optimized data center computational workload at bus n after spatial redistribution.

C. Security and Reserve Constraints

For $N-1$ reliability, spinning reserve r_g for generator g satisfies:

$$P_g + r_g \leq P_g^{\max}, \quad \forall g \in \mathcal{G}, \quad (6)$$

$$r_g \leq RU_g \cdot \Delta T, \quad \forall g \in \mathcal{G}, \quad (7)$$

$$\sum_{m \in \mathcal{G}} r_m \geq P_g + r_g, \quad \forall g \in \mathcal{G}, \quad (8)$$

where RU_g is the ramp-up rate parameter and ΔT is the reserve deployment window. Constraint (6) ensures dispatch plus reserve remain within capacity; (7) limits reserve by ramping capability; (8) guarantees system-wide reserve covers the loss of any unit.

D. Renewable and Flexible Demand Modeling

The solar power output P_n^{solar} at site n is modeled with available maximum power \bar{P}_n^{solar} and curtailment P_n^{curt} :

$$P_n^{\text{solar}} = \bar{P}_n^{\text{solar}} - P_n^{\text{curt}}, \quad (9)$$

$$0 \leq P_n^{\text{curt}} \leq \bar{P}_n^{\text{solar}}, \quad (10)$$

where P_n^{curt} represents the curtailed solar power at site n .

Data center workload flexibility is modeled through the following constraints:

$$L_n^{\text{optimized}} \geq (1 - \beta)L_n^{\text{original}}, \quad \forall n \in \mathcal{N}_{\text{DC}}, \quad (11)$$

$$L_n^{\text{optimized}} \leq L_n^{\text{cap}}, \quad \forall n \in \mathcal{N}_{\text{DC}}, \quad (12)$$

$$\sum_{n \in \mathcal{N}_{\text{DC}}} L_n^{\text{optimized}} = \sum_{n \in \mathcal{N}_{\text{DC}}} L_n^{\text{original}}, \quad (13)$$

where L_n^{original} denotes the original data center load at bus n , $L_n^{\text{optimized}}$ represents the optimized data center load following spatial redistribution, L_n^{cap} is the maximum data center capacity at bus n , β denotes the transferable workload ratio, and $\mathcal{N}_{\text{DC}} \subseteq \mathcal{N}$ represents the set of buses hosting data center loads.

Constraint (11) limits the maximum load reduction at each data center based on workload transferability; (12) enforces the physical capacity limit at each facility; and (13) ensures system-wide conservation of total computational workload.

E. Model Discussion

This formulation (1)–(13) represents a tractable linear programming framework that jointly optimizes energy generation, reserves, renewable curtailment, and flexible load dispatch. The model enables endogenous determination of economic dispatch with renewable spillage under network congestion and security considerations, while utilizing spatial flexibility of data center workloads to alleviate intermittency, moderate price fluctuations, and enhance overall system resilience.

III. CASE STUDIES

This section evaluates spatial DC flexibility impacts on power system operations using a modified IEEE 73-bus test system augmented with three data centers with individual capacity limits of $L_n^{\text{cap}} = 900$ MW. Each optimal power flow (OPF) problem is solved using Gurobi 11.0 under three load scenarios normalized to base load: shoulder (100%), peak (120%), and off-peak (80%). The four studies examine: (1) congestion impacts of inflexible DC deployment, (2) baseline feasibility under fixed DC placement, (3) flexibility threshold requirements, and (4) solar curtailment mitigation through spatial reallocation.

A. Case Study 1: Fixed DC Congestion Impact

This study quantifies the congestion impacts of large-scale DC deployment by comparing the No-DC baseline against Fixed DC configurations. The Fixed DC scenario deploys 1,450 MW total capacity across three strategic locations: 870 MW at Bus 27, 290 MW at Bus 47, and 290 MW at Bus 73.

To diagnose infeasibility arising from concentrated DC loads, an α -relaxation is applied to transmission line capacity constraints. Specifically, equation (4) is updated by:

$$|P_k| \leq \text{RateA}_k + \alpha_k, \quad \alpha_k \geq 0, \quad \forall k \in \mathcal{K} \quad (14)$$

where α_k denotes the virtual capacity (MW) added to branch k to restore feasibility. By penalizing $\sum_k \alpha_k$ in the objective function, this formulation enables analysis under otherwise infeasible DC configurations and quantifies the magnitude of network constraint violations.

Table I quantifies infeasibility through required virtual capacity. The results indicate that Line 47 (Bus 27–33) experiences overload under all three load scenarios, with the peak scenario requiring 52.7 MW of virtual capacity—30.1% above line rating.

TABLE I
BASELINE LINE FLOWS AND FIXED DC INFEASIBILITY (LINE 47: BUS 27–33)

Scenario	Cap. (MW)	No-DC Baseline		Fixed DC	
		Flow (MW)	Util. (%)	Status	α (MW)
Peak	175	71.0	40.6	Infeasible	52.7
Shoulder	175	68.5	39.1	Infeasible	25.1
Off-Peak	175	59.3	33.9	Infeasible	2.1

α : Virtual capacity required for Fixed DC feasibility.

Table II reveals critical capacity violations under Fixed DC deployment. Peak flows reach 227.7 MW, exceeding line capacity by 30.1%, while shoulder and off-peak scenarios exhibit 14.4% and 1.2% overloads, respectively. Spatial DC optimization through load redistribution eliminates all violations, reducing peak utilization to 77.7%, shoulder to 67.0%, and off-peak to 39.7%.

TABLE II
TRANSMISSION LINE LOADING: FIXED VS. OPTIMIZED DC DEPLOYMENT (LINE 47: BUS 27–33)

Scenario	Cap. (MW)	Fixed DC		Optimized DC	
		Flow (MW)	Util. (%)	Flow (MW)	Util. (%)
Peak	175	227.7	130.1	136.0	77.7
Shoulder	175	200.1	114.4	117.2	67.0
Off-Peak	175	177.1	101.2	69.5	39.7

Util.: Utilization percentage relative to line capacity.

Table III summarizes economic impacts across scenarios. Locational Marginal Prices exhibit load-dependent variations, with shoulder and off-peak periods experiencing more pronounced increases due to congestion-induced redispatch requirements.

TABLE III
SYSTEM-WIDE ECONOMIC IMPACT: LMP AND OPERATING COST ANALYSIS

Scenario	No-DC		Fixed DC	Optimized DC	
	Cost (\$)	LMP (\$/MWh)		Cost (\$)	LMP (\$/MWh)
Peak	119,288	74.75	Infeasible	228,058	75.64
Shoulder	62,521	19.64	Infeasible	131,808	74.75
Off-Peak	44,779	15.89	Infeasible	70,009	19.64

The concentration of 870 MW DC capacity at Bus 27 renders Line 47 infeasible under all operating scenarios, with peak conditions requiring 52.7 MW of virtual capacity (30% above line rating). Fixed DC deployment produces capacity overloads ranging from 1.2% to 30.1% across operating conditions. Spatial DC optimization, achieved by strategically redistributing computing loads across multiple network locations, eliminates all transmission violations while maintaining line utilizations between 39.7% and 77.7%. The findings indicate that geographically distributed load allocation could potentially contribute to alleviating transmission constraints and improving the integration of data centers.

B. Case Study 2: Baseline Flexibility Evaluation

Fixed DC locations remain infeasible across all scenarios due to the 870 MW load concentration at Bus 27. In this case study, the minimum flexibility parameter is set to $\beta = 0.5$, allowing each DC to adjust its load by up to half of its initial load. Table IV summarizes the infeasibility diagnosis using the α -relaxation formulation from Eq. (14). Column headers denote: *Line* as the branch index (e.g., “47 (27→33)” indicates Line 47 connecting Bus 27 to Bus 33), and *Violations* as the count of constraints with $\alpha_\ell > 0$.

TABLE IV
BASELINE INFEASIBILITY DIAGNOSIS VIA α -RELAXATION

Scenario	Total Virtual Capacity $\sum \alpha$ (MW)	Violations (#)	Critical Line (ID: From→To)
Peak	52.7	1	47 (27→33)
Shoulder	25.1	1	47 (27→33)
Off-Peak	2.1	1	47 (27→33)

Notes: (1) *Line* denotes the branch index; (2) *From→To* lists connected bus endpoints; (3) *Violations* counts constraints with $\alpha_\ell > 0$.

Figure 1 compares the data center load distributions under fixed and optimized deployment across three operational scenarios. During peak conditions, spatial optimization redistributes loads such that DC₁ reduces from 870 MW to 639 MW, DC₂ decreases to 145 MW, and DC₃ increases to 666 MW. In the shoulder period (base case), DC₁ further decreases to 618.7 MW, DC₂ maintains 145 MW, and DC₃ reaches 686.3 MW. The off-peak scenario exhibits distinct reallocation patterns: DC₁ decreases to 565.6 MW, while DC₂ experiences substantial increase to 657.9 MW and DC₃ reduces to 226.5 MW. All scenarios preserve the total DC load of 1,450 MW as enforced by constraint (13).

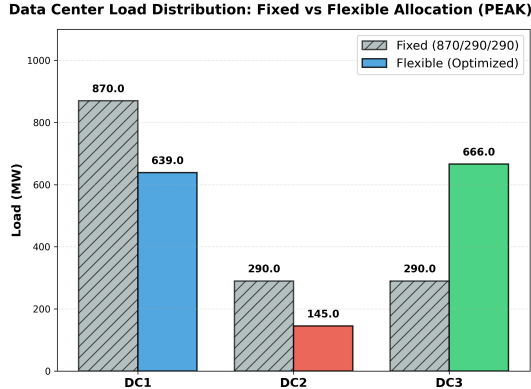


Fig. 1. DC load distribution comparison: Fixed vs. Optimized deployment under flexibility constraints.

The congestion relief achieved through spatial reallocation ranges from 2.1 MW (off-peak) to 52.7 MW (peak), as quantified by the $\sum \alpha$ metric in Table IV. Line 47 connecting Buses 27 and 33 consistently emerges as the critical transmission bottleneck across all operating conditions.

C. Case Study 3: Flexibility Threshold Analysis

This study analyzes the impact of the DC transferable workload ratio (β), varying from $\beta = 0.1$ to $\beta = 0.5$, on a modified IEEE 73-bus system to identify economic thresholds and diminishing returns. The system includes three DCs totaling 1,450 MW (870 MW at Bus 27; 290 MW each at Buses 47 and 73). Scenarios for β values of 0.1, 0.2, 0.3, 0.4, and 0.5 were simulated under peak, shoulder, and off-peak loads using Gurobi 11.0. Table V shows total system costs declining as β increases, confirming diminishing returns. All scenarios are feasible at the $\beta = 0.1$ limit. The Peak scenario's cost saturates at $\beta = 0.2$, saving \$3,794 compared to $\beta = 0.1$. The Shoulder scenario also saturates at $\beta = 0.2$, saving a more modest \$135. In contrast, the Off-Peak scenario requires $\beta = 0.3$ to reach saturation, achieving a total savings of \$4,913. This demonstrates that the economic saturation point for flexibility is load-dependent.

TABLE V
TOTAL SYSTEM COST UNDER VARYING DC TRANSFER LIMITS

Transfer Limit (β)	Peak (\$)	Shoulder (\$)	Off-Peak (\$)
$\beta = 0.1$	231,852.40	131,942.55	74,922.17
$\beta = 0.2$	228,057.73	131,808.16	70,094.19
$\beta = 0.3$	228,057.73	131,808.15	70,008.95
$\beta = 0.4$	228,057.73	131,808.15	70,008.95
$\beta = 0.5$	228,057.73	131,808.16	70,008.95

The corresponding system-wide LMP response is illustrated in Fig. 2. While increased flexibility (higher β) generally lowers LMPs by resolving congestion, a counter-intuitive dynamic emerges. The Off-Peak scenario (blue triangles) shows LMP reduction from \$19.64/MWh to \$13.53/MWh as β increases from 0.1 to its 0.3 saturation point, and the Peak (red circles) drops from \$87.64/MWh to \$74.75/MWh from $\beta = 0.1$ to $\beta = 0.2$. However, the Shoulder scenario (green squares) behaves differently.

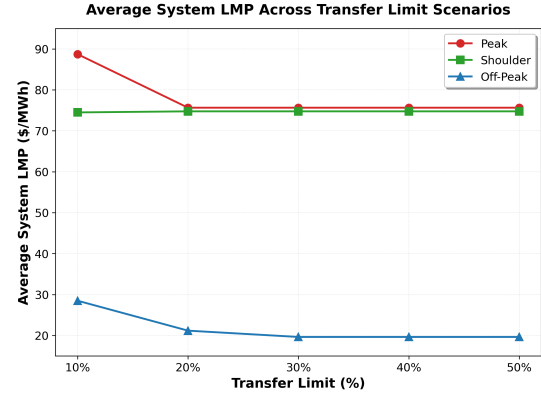


Fig. 2. Average System LMP Across Transfer Limit Scenarios

Notably, a counter-intuitive dynamic emerges in the Shoulder scenario: the average LMP slightly increases from \$74.49/MWh (at $\beta = 0.1$) to \$74.75/MWh (at $\beta = 0.2$). Critically, the Total System Cost correctly decreases (per Table V), confirming the $\beta = 0.2$ case is economically superior. The LMP behavior is explained by congestion relief. At $\beta = 0.1$, the system is congested due to insufficient flexibility. This creates multiple price zones, and the \$74.49/MWh is merely an average of these disparate prices. At $\beta = 0.2$, the added flexibility resolves the bottleneck, moving the system to an uncongested state. Consequently, all nodes clear at a single, unified marginal price of \$74.75/MWh.

The β value required for LMP saturation is scenario-dependent, as shown by the curves flattening in Fig. 2. Peak and Shoulder scenarios stabilize at $\beta = 0.2$, while Off-Peak requires $\beta = 0.3$. This finding illustrates that lower system loads do not necessarily correlate with a reduced need for flexibility to reach an uncongested, optimal economic state.

D. Case Study 4: Solar Curtailment Management

The modified IEEE 73-bus system incorporates 2,800 MW of solar PV generation located near congested transmission corridors (buses 27 and 33), reflecting practical renewable integration challenges. Three data centers with a total demand of 1,450 MW are included, each permitted to shift up to 50% of its initial load to alternate locations ($\beta = 0.5$). Two operational configurations are analyzed: Fixed DC, representing inflexible deployment, and Optimized DC, which enables spatial reallocation toward solar-abundant buses.

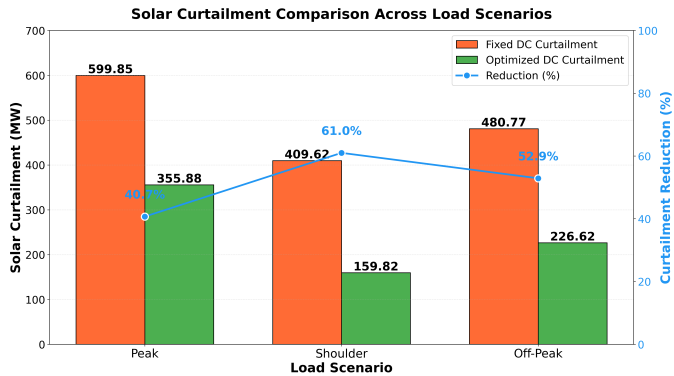


Fig. 3. Solar curtailment comparison across load scenarios under fixed and optimized DC operation.

Quantitative results across three loading scenarios (peak, shoulder, and off-peak) are summarized in Fig. 3. Under the Fixed DC configuration, total curtailed solar generation reached 599.85 MW, 409.62 MW, and 480.77 MW for the peak, shoulder, and off-peak conditions, respectively. These curtailments mainly resulted from transmission bottlenecks near buses 27 and 33 that restricted power transfer from local PV plants. With spatially Optimized DC operation, curtailed solar generation decreased to 355.88 MW, 159.82 MW, and 226.62 MW under the same conditions. The reductions relative to the Fixed DC configuration were 40.7%, 61.0%, and 52.9%, demonstrating that optimized spatial load reallocation enhances the utilization of locally generated solar power constrained by transmission limits.

IV. CONCLUSION

This paper presented a OPF framework to evaluate the potential of spatially flexible data centers on a modified IEEE 73-bus system. The findings indicate that while inflexible, concentrated DC deployment can lead to severe transmission violations (up to 30.1% overload) and system infeasibility, enabling spatial flexibility can help mitigate these issues. In the studied scenarios, strategic workload reallocation was found to mitigate these violations, restore feasibility, and contribute to a notable reduction in solar curtailment (by up to 61.0%) by shifting load to solar-rich areas. We also identified an economic saturation point, finding that 20 to 30% workload transferability appears to capture the majority of operational cost savings. These results suggest that spatially flexible DCs could serve as a viable resource, potentially deferring or replacing traditional transmission network upgrades.

While this study provides a deterministic validation, future work should extend this framework. This includes incorporating the stochastic nature of renewable forecasts, integrating unit commitment logic, and analyzing coupled transmission-distribution coordination [18]–[20]. Such extensions are essential for developing practical, co-optimized flexibility resources to support deep decarbonization pathways.

REFERENCES

- [1] Y. Ran, H. Hu, Y. Wen and X. Zhou, “Optimizing energy efficiency for data center via parameterized deep reinforcement learning,” *IEEE Trans. Serv. Comput.*, vol. 16, no. 2, pp. 1310–1323, Mar.–Apr. 2023, doi: 10.1109/TSC.2022.3184835.
- [2] J. Gao et al., “A data load spatio-temporal scheduling method considering thermal inertia in data centres,” in *Proc. IEEE Int. Conf. Elect. Energy Convers. Syst. Control (IEECSC)*, Chongqing, China, 2025, pp. 332–336, doi: 10.1109/IEECSC64206.2025.11099787.
- [3] S. Zhang, J. Lyu, W. Jin, H. Cheng, C. Li and X. Wang, “Coordinated planning of multiple energy hubs considering the spatiotemporal load regulation of data centers,” *IEEE Trans. Power Syst.*, vol. 39, no. 2, pp. 4193–4207, Mar. 2024, doi: 10.1109/TPWRS.2023.3296101.
- [4] J. Silva-Rodriguez, E. Raffoul and X. Li, “LSTM-based net load forecasting for wind and solar power-equipped microgrids,” in *Proc. 56th North Amer. Power Symp. (NAPS)*, El Paso, TX, USA, 2024, pp. 1–6, doi: 10.1109/NAPS61145.2024.10741801.
- [5] X. Fang, B.-M. Hodge, E. Du, C. Kang and F. Li, “Introducing uncertainty components in locational marginal prices for pricing wind power and load uncertainties,” *IEEE Trans. Power Syst.*, vol. 34, no. 3, pp. 2013–2024, May 2019, doi: 10.1109/TPWRS.2018.2881131.
- [6] A. L. Figueroa-Acevedo, C.-H. Tsai, K. Gruchalla, Z. Claes, S. Foley and J. Bakke, “Visualizing the impacts of renewable energy growth in the U.S. midcontinent,” *IEEE Open Access J. Power Energy*, vol. 7, pp. 91–99, 2020, doi: 10.1109/OAJPE.2020.2967292.
- [7] F. Jiang, X. Li and P. Van Hentenryck, “A Deep Neural Network-based Frequency Predictor for Frequency-Constrained Optimal Power Flow,” in *Proc. IEEE Ind. Appl. Soc. Annu. Meeting (IAS)*, Taipei, Taiwan, 2025, pp. 1–5, doi: 10.1109/IAS62731.2025.11061730.
- [8] T. Pham and X. Li, “Reduced Optimal Power Flow Using Graph Neural Network,” in *Proc. North Amer. Power Symp. (NAPS)*, Salt Lake City, UT, USA, 2022, pp. 1–6, doi: 10.1109/NAPS6150.2022.10012256.
- [9] U.S. Department of Energy, “Electricity demand growth resource hub,” [Online]. Available: <https://www.energy.gov/policy/electricity-demand-growth-resource-hub>. Accessed on: Nov. 1, 2025.
- [10] B. L. Tarufelli et al., “Price formation and grid operation impacts from variable renewable energy resources.” U.S. Dept. Energy, Washington, DC, USA, Rep. DOE/NETL-2022/3271, Sep. 2022, doi: 10.2172/1993624.
- [11] U.S. Energy Information Administration, “What is U.S. electricity generation by energy source?” [Online]. Available: <https://www.eia.gov/tools/faqs/faq.php?id=427&t=3>. Accessed on: Nov. 1, 2025.
- [12] J. Dong, J. Zhang and L. Shi, “Evaluation of transmission expansion benefits in competitive power market,” in *Proc. 3rd Int. Conf. Electric Utility Deregulation and Restructuring and Power Technologies (DRPT)*, Nanjing, China, 2008, pp. 1216–1220, doi: 10.1109/DRPT.2008.4523592.
- [13] Z. Chen, L. Wu and Z. Li, “Electric demand response management for distributed large-scale internet data centers,” *IEEE Trans. Smart Grid*, vol. 5, no. 2, pp. 651–661, Mar. 2014, doi: 10.1109/TSG.2013.2267397.
- [14] H. Wang, J. Huang, X. Lin and H. Mohsenian-Rad, “Proactive demand response for data centers: A win-win solution,” *IEEE Trans. Smart Grid*, vol. 7, no. 3, pp. 1584–1596, May 2016, doi: 10.1109/TSG.2015.2501808.
- [15] Y. Zhang, D. C. Wilson, I. C. Paschalidis and A. K. Coskun, “HPC data center participation in demand response: An adaptive policy with QoS assurance,” *IEEE Trans. Sustain. Comput.*, vol. 7, no. 1, pp. 157–171, Jan.–Mar. 2022, doi: 10.1109/TSUSC.2021.3077254.
- [16] M. H. Hajiesmaili, D. Cai and E. Mallada, “Understanding the inefficiency of security-constrained economic dispatch,” in *Proc. IEEE 56th Annu. Conf. Decision Control (CDC)*, Melbourne, VIC, Australia, 2017, pp. 2035–2040, doi: 10.1109/CDC.2017.8263947.
- [17] G. Fridgen, R. Keller, M. Thummel and L. Wederhake, “Shifting load through space—The economics of spatial demand side management using distributed data centers,” *Energy Policy*, vol. 109, pp. 400–413, Oct. 2017, doi: 10.1016/j.enpol.2017.07.018.
- [18] Q. P. Zheng, J. Wang and A. L. Liu, “Stochastic optimization for unit commitment—A review,” *IEEE Trans. Power Syst.*, vol. 30, no. 4, pp. 1913–1924, Jul. 2015, doi: 10.1109/TPWRS.2014.2355204.
- [19] U. Cetinkaya, R. Bayindir and S. Ayik, “Ancillary services using battery energy systems and demand response,” in *Proc. 9th Int. Conf. Smart Grid (icSmartGrid)*, Setubal, Portugal, 2021, pp. 212–215, doi: 10.1109/icSmartGrid52357.2021.9551253.
- [20] G. Liu and K. Tomovic, “A full demand response model in co-optimized energy and reserve market,” *Elect. Power Syst. Res.*, vol. 111, pp. 62–70, Jun. 2014, doi: 10.1016/j.epsr.2014.02.006.